Applied Surface Science 508 (2020) 145140

Contents lists available at ScienceDirect

Applied Surface Science

journal homepage: www.elsevier.com/locate/apsusc

Full Length Article

Effects of laser-induced periodic surface structures on the superconducting properties of Niobium

A. Cubero[a], E. Martínez[a], L.A. Angurel[a,*], G.F. de la Fuente[a], R. Navarro[a], H. Legall[b], J. Krüger[b], J. Bonse[b]

[a] ICMA (CSIC-University of Zaragoza), c/María de Luna 3, 50018 Zaragoza, Spain
[b] Bundesanstalt für Materialforschung und –prüfung (BAM), Unter den Eichen 87, 12205 Berlin, Germany

ARTICLE INFO

Keywords:
LIPSS
Femtosecond n-IR laser
Sub-nanosecond UV laser
Niobium
Superconductivity

ABSTRACT

It is well known that the use of ultrashort (fs) pulsed lasers can induce the generation of (quasi-) periodic nanostructures (LIPSS, ripples) on the surface of many materials. Such nanostructures have also been observed in sample's surfaces irradiated with UV lasers with a pulse duration of 300 ps. In this work, we compare the characteristics of these nanostructures on 1-mm and on 25-μm thick niobium sheets induced by 30 fs n-IR and 300 ps UV pulsed lasers. In addition to conventional continuous or burst mode processing configurations, two-dimensional laser beam and line scanning modes have been investigated in this work. The latter allows the processing of large areas with a more uniform distribution of nanostructures at the surface. The influence of the generated nanostructures on the superconducting properties of niobium has also been explored. For this aim, magnetic hysteresis loops have been measured at different cryogenic temperatures to analyse how these laser treatments affect the flux pinning behaviour and, in consequence, the superconductor's critical current values. It was observed that laser treatments are able to modify the superconducting properties of niobium samples.

1. Introduction

The generation of laser-induced periodic surface structures (LIPSS) is observed in many materials when their surface is irradiated using a linearly polarized laser [1,2]. In the last years the number of theoretical and experimental works increases continuously. Further on, it has been observed that these nanostructures feature new surface properties that are very useful in a wide range of applications, such as control of the colour [3], iridescence [3,4], wettability [5] or antibacterial properties [6], for example. Among the different laser processing parameters, the local fluence has been proven to influence strongly the morphology of the generated LIPSS, whose periodicity and orientation is also determined by the laser wavelength and the polarization. Besides, it has been observed that the laser incidence angle, the crystal orientation of the grains of the irradiated material, the presence of local defects, as well as the surface roughness can also modify the characteristics of these nanostructures [7–9].

Niobium is the pure metal presenting type II superconductivity with the highest critical temperature T_c = 9.28 K and critical magnetic fields [10]. It also may reach low microwave surface resistance, and therefore it is used to improve the efficiency of superconducting radio frequency (SRF) cavities in particle accelerators [11]. The quality of Nb SRF resonators is strongly affected by the surface properties [12–14]. In addition to morphology issues, surface studies reveal the presence of oxides, hydrides and groups of hydrocarbons in the surface of high-purity niobium materials [15]. Commonly, chemical polishing or electrolytic polishing are used to reduce roughness and to remove surface contamination in order to improve the performance of Nb SRF cavities. Furthermore, niobium alloys have been used in the last decades in the fabrication of superconducting coils. In type II superconducting materials, magnetic fields above a certain threshold field value, named *lower critical field* (H_{c1}), penetrate the material forming a lattice of quantized line vortices. Upon increasing the magnetic field, the number of vortices increases and the distance between them reduces. Finally, at an *upper critical field* H_{c2}, the vortex lattice collapses and the bulk superconducting state disappears. At intermediate magnetic fields, when a current is applied to the superconductor, a Lorentz force acts on the vortices, which may cause them to move generating a dissipative voltage. To avoid this, a network of defects has to be generated in the superconductor to locally pin the vortex lattice.

The potential use of ultrashort laser pulse sources for high-speed manufacturing of periodic nanostructures (LIPSS) as pure surface

* Corresponding author.
E-mail address: angurel@unizar.es (L.A. Angurel).

https://doi.org/10.1016/j.apsusc.2019.145140
Received 18 September 2019; Received in revised form 7 December 2019; Accepted 19 December 2019
Available online 20 December 2019

defects and how they can modify the surface characteristics, and in consequence, the superconducting properties, is the main aim of this research. With this aim in mind, an analysis of the different surface morphologies that can be generated by fs n-IR and ps UV lasers on the Nb surfaces, both in beam and line scan mode [16,17] is presented in this paper. Representative samples were chosen in order to check whether the superconducting properties of the laser treated samples had been modified in comparison with the original ones.

2. Experimental

Laser irradiation experiments have been performed on 1-mm thick Nb sheets (99.9% purity, Goodfellow) and on 25-μm thick Nb foils (99.8% purity, Alfa Aesar) with a surface micro-roughness of 0.25 μm. A picosecond UV laser (Rofin-Sinar - wavelength $\lambda = 355$ nm, pulse duration $\tau_p = 300$ ps, $1/e^2$ beam diameter $D_b = 34$ μm, and pulse repetition frequencies $f = 250$–800 kHz) and a femtosecond n-IR Ti:Sapphire laser (Femtolasers Compact Pro - wavelength $\lambda = 790$ nm, pulse duration $\tau_p = 30$ fs, $1/e^2$ beam diameter $D_b = 130$ μm, and pulse repetition frequency $f = 1$ kHz) were used to scan the surface of the samples.

In the ps UV laser facility, the beam is moved using an optical beam steering system at a given speed, using two different scanning protocols: *i*) *Beam scanning mode*. The sample has a fixed position and the laser scans across the surface, controlling the overlapping between successive laser scans. *ii) Line scanning mode*. The laser spot moves in a given direction writing a line of length l_L for a given number of times, while the sample is moving in the perpendicular direction. In this mode, the distance between two laser-line scans is controlled by adjusting the laser scanning speed, the length of the line and the sample traverse speed.

In the fs n-IR laser facility, the laser beam focus position is fixed and the sample describes a meandering movement in two perpendicular directions. In one direction the sample velocity is set constant in order to control the spatial overlapping between successive laser dots, while in the other orthogonal direction, the distance between successive lines is also controlled.

Using the ps UV laser, the sample can be placed inside a processing chamber and the laser goes in through an optical window allowing the control of the gas atmosphere during the laser treatment. In 1 mm thick samples the irradiation was performed in N_2 atmosphere, while the 25 μm thick samples were processed in ambient air in order to have similar processing conditions with both laser systems.

The generated surface nanostructures are imposed by the individual characteristics of each laser beam, but also by cumulative effects due to the overlapping of successive laser spots along a line and the lateral distance between successive lines [18,19]. In order to characterize the laser treatments, several parameters have been defined:

Pulse fluence: Energy per unit area of a given pulse, $F_p = (P/f)/A_b$, where P is the average laser power, f is the pulse repetition frequency and A_b the cross-section of the laser beam at the sample.

Pulse irradiance: Power per unit area of a given pulse, $I_p = F_p/\tau_p$, where τ_p is the pulse duration.

Effective number of pulses in a line: The effective number of pulses received by any point of the surface scanned in an isolated line is given by $N_L = D_b/d_b = D_b f/v_L$, where d_b is the displacement of two successive dot centres and, v_L the laser beam scanning velocity. N_L is a measure of the number of pulses that overlap and has manufacture relevance because it controls the homogeneity of the total fluence along the line.

Average cumulative energy per unit area in a line, F_L: Total energy per unit area when laser beam scans in one direction taking into account the average fluence of the individual pulse and the pulse to pulse overlap in this direction, $F_L = N_L F_b$.

Effective number of line scans. The effective number of scans that affect any point of the final scanned surface is given by $N_S = D_b/d_s$, where d_s corresponds to the distances of the centres of two successive scanning lines. If the laser line scan mode is used, v_s defines the sample velocity and t_s the time that the laser needs to completely scan a line, $N_S = D_b/d_s = D_b/(v_s t_s)$. N_S controls the total fluence homogeneity in the direction perpendicular to the scanned lines.

The surface morphology of the irradiated samples was analysed by scanning electron microscopy (SEM) in a field-emission scanning electron microscope (FE-SEM, Carl Zeiss MERLIN) using secondary electrons (SE) and in-lens secondary electron detectors. Nanostructure periodicity has been determined by measuring in several regions of the images the distance to cover several consecutive periods. Chemical surface characterization was performed by energy dispersive X-ray analysis (EDX, INCA350 Oxford Instruments) employing electron acceleration voltages of 5 kV. Atomic force microscopy (AFM) measurements were performed with a scanning probe microscope (SPM) Ntegra Aura system of NT-MDT. The analysis of the AFM measurements was carried out using Gwyddion software (version 2.53). Finally, the superconducting properties of selected samples were analysed using a SQUID-based Quantum Design MPMS-5T system performing DC magnetic $M(H)$ measurements at constant temperature in zero magnetic field cooling conditions. For the latter purpose, the representative samples studied were cut in rectangular shape with dimensions ranging between 3 and 4 mm.

3. Initial experiments in 1-mm thick Nb samples

Initial experiments were performed on 1-mm thick samples. Before laser treatments, sample surfaces were polished with sand paper and Al_2O_3–based polishing suspensions. Samples C1 and C2 were processed with the 300 ps UV laser inside the chamber in a N_2 atmosphere (1.4 atm) with the particular parameters recorded in Table 1. The samples showed here have been processed using the laser *line scanning mode* [16,17] with a sample traverse velocity of $v_s = 0.04$ mm/s that would be equivalent to a *beam scanning mode* with $d_s = 5$ μm. The pulse irradiance I_p was set to similar vales in both samples, but the higher N_L gives laser conditions slightly more intense for sample C2.

Fig. 1 shows the typical nanostructures obtained in these samples after the applied laser surface treatment. Sample C1 (Fig. 1a) exhibits rippled nanostructures with spatial periodicity $\Lambda_{LIPSS} = 276 \pm 13$ nm, between the neighbouring nanostructures observed in the SEM micrograph. This value is very close to the laser wavelength, and the orientation of these structures is almost perpendicular to the laser polarization direction. It should be pointed out that the structure of the ripples is not smooth, but accompanied by some drop-like protrusions that appear in the SEM micrographs as small circles. Their appearance is consistent with the melting of a thin layer of the sample during the laser scanning and the alignment of small volumes (micro-drops) of molten material with the ripples. Sample C2 (Fig. 1b), processed with slightly more intense conditions, also presents well-defined nano-protrusions along the ripples, with $\Lambda_{LIPSS} = 294 \pm 8$ nm, similar to sample C1. It should be remarked that those of nearest ripples interact, inducing a certain degree of order in the direction perpendicular to the ripples.

EDX measurements indicate that, during the laser treatment with the ps UV laser in a N_2 atmosphere, the amount of oxygen in the surface of the sample is slightly reduced. Before laser treatment, the ratio O/Nb in atomic percentage is 0.41 ± 0.05, a value that reduces down to

Table 1
Laser processing parameters used on 1-mm thick Nb samples irradiated with the ps UV laser in N_2 atmosphere.

Sample	P (W)	f (kHz)	v_L (mm/s)	d_s (μm)	I_p (GW/cm^2)	N_L	N_S
C1	0.85	700	300	5	0.45	79	7
C2	1	800	300	5	0.46	91	7

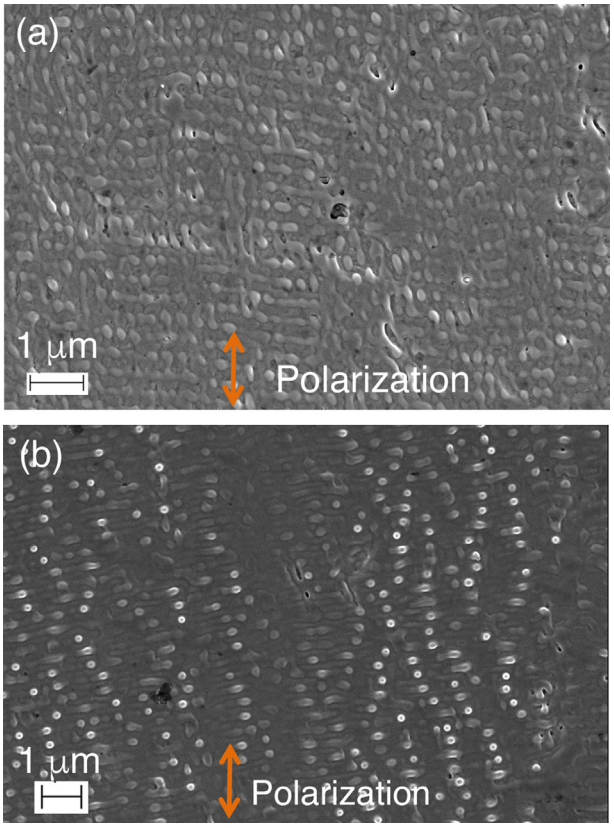

Fig. 1. Nanostructures obtained in 1-mm thick Nb samples C1 (a) and C2 (b) processed in N_2 atmosphere. The arrows indicate the laser polarization direction.

0.34 ± 0.01 after laser interaction.

Self-organized multiscale surface structures similar to those presented in Fig. 1 have been observed in thin films of metals [20] and oxides [21] deposited on glass and on metallic sheets. These were observed upon irradiation by superposition, on the same spot, of series of tens to hundreds of UV laser shots with fs and ps pulse duration. In some cases, these structures were also observed in larger areas obtained by laser beam scanning [21]. This self-organization may be affected by the minimization of the free-surface energy, needs the presence of a fluid phase (molten material) and evolves with the number of shots. In our case, this fluid phase is easily obtained due to the higher pulse duration, the high absorption coefficient and the low penetration depth that characterize the interaction with the UV radiation [22]. When the temperature changes substantially along the target surface, the gradients of the surface tension, $\nabla\gamma$, result in thermocapillary forces, which can move the fluid from the hot regions to the cold ones. This phenomenon is known as the Marangoni effect or capillary motion [23]. These gradients produce the flow of molten liquids away from areas with higher laser intensity. The self-organized structures evolve with the overlap of subsequent pulses.

The effect of the generated periodic surface nanostructures on the superconducting properties of Nb can be analysed from the magnetic hysteresis curves, $M(H)$. Fig. 2a compares the measured curves at $T = 8$ K for a sample whose top and bottom surfaces were irradiated with laser conditions C1, and for a polished non-treated reference (original) sample. In the first quadrant of Fig. 2a, the $M(H)$ dependence in the original sample is linear in a broad range of magnetic field values, whereas in the laser treated C1 sample, a small kink at about 0.05 T is observed. It is important to recall here that the width of the magnetic hysteresis loops, $\Delta M(H)$, which is defined as the difference between the descending- and the ascending-branch magnetization, is proportional to the critical current density, $J_c(H)$ [24,25]. J_c is

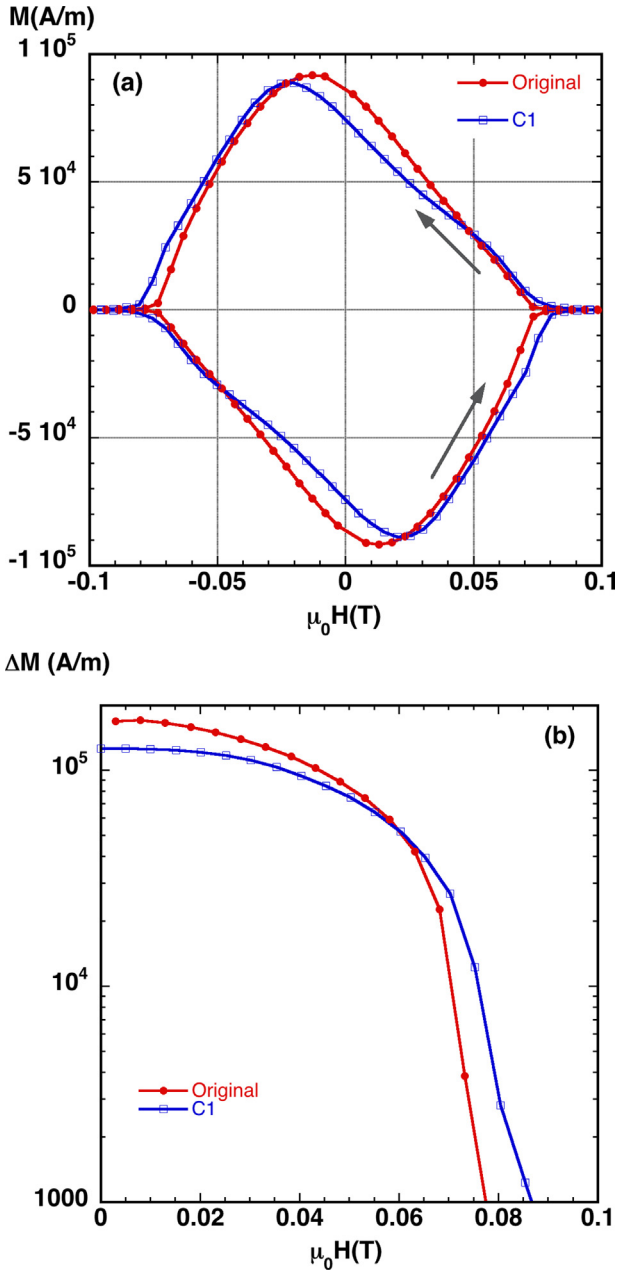

Fig. 2. (a) Magnetic hysteresis loops measured at 8 K in an original reference sample and in sample C1 of 1-mm thickness. The magnetic field, H, was applied perpendicular to the surfaces. Arrows indicate field sweep directions. (b) Magnetic field dependence of the width of hysteresis loops, $\Delta M(H)$, of the same samples, calculated as explained in text.

determined by the ability of the material to trap vortices (flux vortex pinning) and therefore it is strongly dependent on the material defects structure that are able to pin the vortices, such as nano-sized impurities, dislocations or grain boundaries. Fig. 2b compares the $\Delta M(H)$ curves for both samples. It is clearly observed that the ps-laser treatment has produced some changes in the superconducting properties of the processed sample compared to the reference one, with a small reduction of the ΔM values at low fields, and an increase at magnetic fields above 0.6 T. Obviously, the ps-laser treatment only affects a very thin surface layer, whereas ΔM values are also associated to bulk pinning effects. For this reason, we decided to continue this work in 25 μm thick samples, in order to improve the ratio between surface and bulk effects.

Table 2
Laser processing parameters used in 25 μm thick Nb samples irradiated with the fs n-IR and with the ps UV lasers (FS and PS, respectively).

Sample	*P* (W)	*f* (kHz)	v_L (mm/s)	d_s (μm)	F_p (J/cm^2)	I_p (GW/cm^2)	N_L	N_S
FS1	0.012	1	6	20	0.09	3014	20	7
FS2	0.015	1	6	20	0.11	3767	20	7
FS3	0.020	1	6	20	0.15	5023	20	7
PS1	0.5	600	600	5	0.1	0.32	34	7
PS2	1.1	300	300	7	0.4	1.35	34	5
PS3	1.1	300	300	3	0.4	1.35	34	11

4. Comparison of nanostructures in 25 μm thick foils using fs n-IR and ps UV lasers

A systematic search of different nanostructures generated on the Nb surface by irradiation with these two laser systems has been done. Due to the large difference in the pulse duration in both lasers, the pulse irradiance is three orders of magnitude higher for the fs n-IR laser and only comparisons of samples with similar fluence values are possible. In addition, due to the difference in pulse duration, thermal processes are more relevant when the ps UV laser is used. The laser parameters used in the processing of the samples analysed in this contribution are compiled in Table 2.

4.1. Nanostructures generated with the fs n-IR and ps UV laser

The top-view SEM micrographs collected in Fig. 3 compare the surface microstructures of the samples chosen in Table 2. Furthermore, details of some of these nanostructures are presented in Fig. 4. In the case of the samples processed with the fs n-IR laser, surface modification starts when a pulse fluence of 0.09 J/cm^2 is reached (Fig. 3a). The initial features generated on the irradiated samples are small surface structures, parallel to the laser polarization direction with a periodicity close to 40 nm (Fig. 4a). This structure can be considered as a type of high spatial frequency LIPSS (HSFL). When the pulse fluence increases up to 0.11 J/cm^2, the typical low spatial frequency LIPSS (LSFL) that

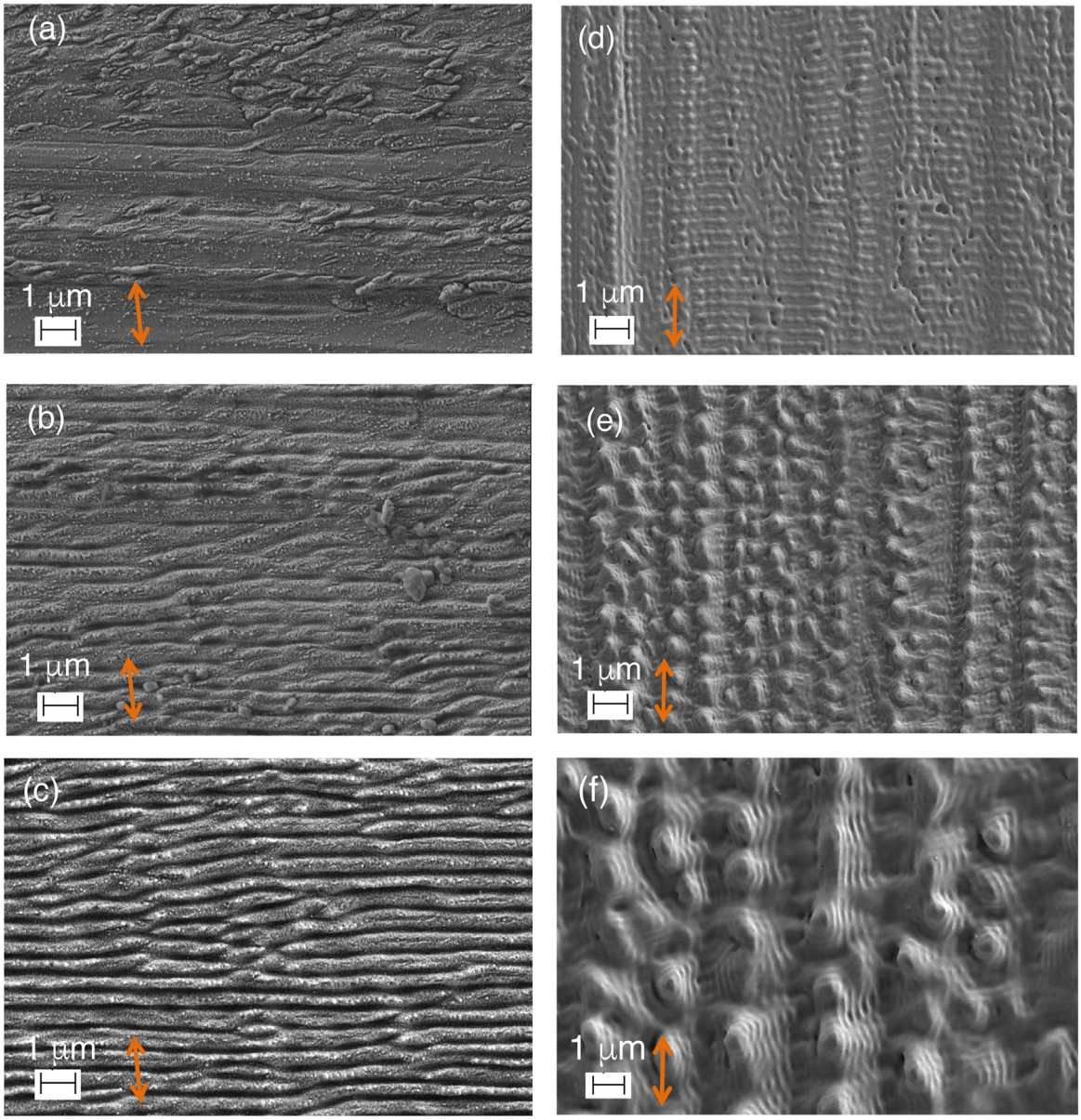

Fig. 3. SEM images showing the nanostructures obtained in 25-μm thick Nb foils processed with the fs n-IR laser: samples FS1 (a), FS2 (b) and FS3 (c) and with the ps UV laser: samples PS1 (d), PS2 (e) and PS3 (f). The arrows indicate the laser polarization direction.

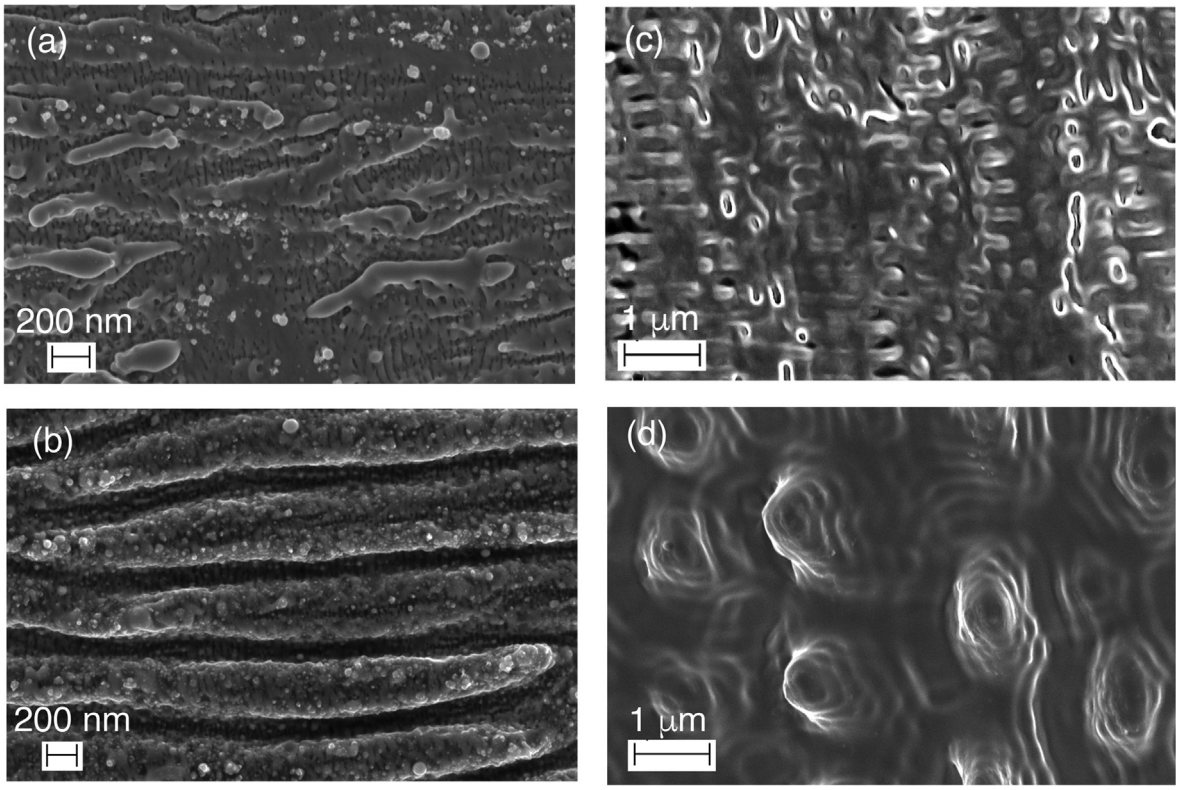

Fig. 4. SEM micrographs showing details of the nanostructures generated in some of the samples: FS1 (a), FS3 (b), PS1 (c) and PS3 (d) shown in Fig. 3.

are observed in many metals [2,26] and in Nb [27], in particular when irradiated with fs laser pulses, have been generated (Fig. 3b). The HSFL nanostructures observed in sample FS1 are detected between two of these LSFL structures. Increasing the irradiance, these LSFL are more pronounced at the surface (Figs. 3c and 4b). The images clearly show that melting effects are negligible with this laser. With the low pulse repetition frequency (1 kHz), the time between two consecutive laser pulses is 1 ms, much larger than the typical relaxation times (10–30 ps). In consequence, once a given fluence threshold is surpassed, an individual pulse modifies the surface, as well as the material absorption for the following pulse.

The UV laser is characterized by a pulse duration of 300 ps. In consequence, thermal processes are relevant. In addition, this laser system operates at high pulse repetition frequencies and, in consequence, the time between two consecutive pulses is in the range of 1–4 μs. Furthermore, the time between two scanning lines is in the order of 1–10 ms. For the nanostructure generation process the cumulative effect of the different pulses during a given line scan is the main parameter that defines the final surface structure. The generated nanostructure modifies the laser absorption during the next laser scan cycle, slowly changing the aspect of the final surface nanostructure. It has been established that the minimum value of F_L to generate nanostructures here is 2.26 ± 0.07 J/cm^2.

Fig. 3(d–f) shows the surfaces of the three samples collected in Table 2. Sample PS1 (Figs. 3d and 4c), which has been processed with a value of F_L = 3.31 J/cm^2, close to the LIPSS threshold, exhibits a ripple nanostructure. In case of samples PS2 (Fig. 3e) and PS3 (Figs. 3f and 4d), the pulse repetition frequency has been reduced to 300 kHz. Using similar laser power levels, the pulse fluence and, in consequence, the pulse irradiance values are increased and F_L reaches values of 13.73 J/cm^2. These conditions generate new structures, denominated here as microprotrusions, with distances between two maxima in the order of 1–2 μm. In the case of sample PS2 (N_S = 5), the laser irradiation conditions produce a structure that is intermediate between the ripples and the microprotrusions that are predominant in sample PS3 (N_S = 11). Fig. 4d also shows that inside these protrusions there is a nanostructure with a periodicity very close to the UV laser wavelength.

The characteristics of the different surface nanostructures generated by fs n-IR and ps UV laser irradiation have been further analysed by AFM measurements in samples FS3 and PS1. The results shown in Fig. 5 correspond to AFM topographies and their corresponding line profiles obtained for samples FS3 (upper figures) and PS1 (lower figures). It can be seen that the structures of the FS3 sample have a periodicity of 515 ± 70 nm, approximately 65% of the laser wavelength, and a depth of 150 ± 25 nm (distance between peak to valley). Sample PS1 exhibits a periodicity of 337 ± 25 nm, very close to the used UV laser wavelength (355 nm), and the ripples have considerably lower depth values (18 ± 5 nm) than for sample FS3. It is worth noting that the structure of line profiles is quite different in both cases, since for sample PS1, valleys and peaks are very similar following a sinusoidal-type curve, whereas sample FS3 shows rather flat peaks with sharper valleys. The different characteristics of the generated periodic structures, with elongated grooves for fs n-IR laser irradiated samples that contrasts with the two-dimensional periodicity for the sample irradiated with ps UV laser, can be clearly observed in the insets of Fig. 5a and c. These show 2D-Fourier transforms of the AFM surface area images of samples FS3 and PS1, respectively.

4.2. Comparison of the superconducting behaviour of samples processed with the two lasers

Fig. 6 represents the $\Delta M(H)$ curves as a function of the applied magnetic field for the 25 μm-thick irradiated FS3 and PS1 samples, together with the results obtained for an original reference, nontreated sample, for comparison. These values were obtained as explained in Section 3 from $M(H)$ hysteresis loops measured at 7 K, applying the magnetic field perpendicular to the irradiated surfaces. Note that both the top and bottom surfaces of the samples were irradiated with the laser. It can be seen that the laser irradiation produces changes in the superconducting properties of the samples. An increase of ΔM values is

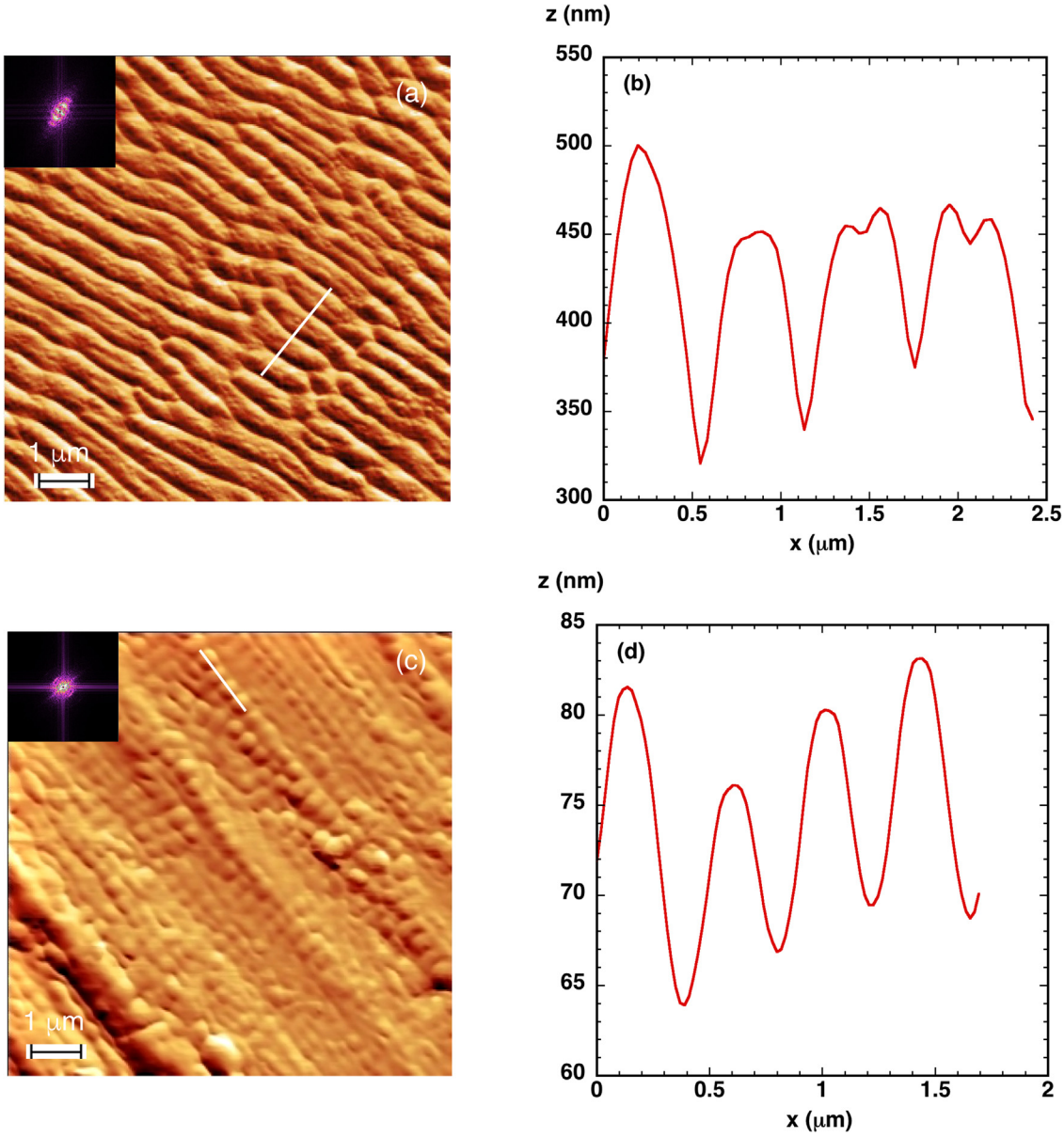

Fig. 5. AFM topography (a, c) and line profile (b, d) of samples FS3 (a, b) and PS1 (c, d). Insets in (a) and (c) are the 2D-Fourier transforms of the corresponding AFM images and the lines mark the regions where the profiles have been measured.

thus observed in sample FS3 for $\mu_0 H < 0.1$ T, whereas a decrease is observed for sample PS1. These results show that laser processing is able to modify the superconducting properties of Nb films either by introducing new defects that are able to create additional vortex pinning centres, or by producing a decrease in the number of vortex pinning centres (cleaner surface). The strong change in the irradiance of both used lasers, which are three orders of magnitude higher for FS than for PS samples, produces surface structures one order of magnitude deeper in the former case. Since a larger depth of material near the surface is affected, more effective pinning is expected for FS samples, in agreement with the results shown in Fig. 6. The observed differences in ΔM imply that surface flux pinning plays an important role in Nb [12]. This behaviour thus suggests that the laser surface treatments herewith presented open new possibilities to control the pinning properties of Nb thin samples in large areas, offering the potential for scale-up to continuous manufacture processes.

5. Conclusions

Differences in pulse width and in pulse repetition frequency values between the fs n-IR and the ps UV lasers employed in this study induce sample irradiation conditions where laser pulse irradiance values differ by more than three orders of magnitude. The latter induce very different nanostructures in Nb foil surfaces. When the fs n-IR laser is used, the nanostructures observed evolve from a HSFL to a LSFL type. In the case of the ps UV laser, the induced surface features initially appear with a ripple nanostructure where some nanoprotrusions start to form and evolve, as the laser intensity is increased, into micro-protrusions. The use of a laser line scanning configuration allows obtaining uniform nanostructures in large areas.

The study of magnetic properties proves that the laser irradiated samples exhibit slightly higher critical current density values in a particular range of magnetic fields, in comparison with reference non-treated samples. This is observed even in the case of 1 mm thick samples, thus opening the possibility to develop a simple, dry and scalable method for improving superconductors at the manufacture level.

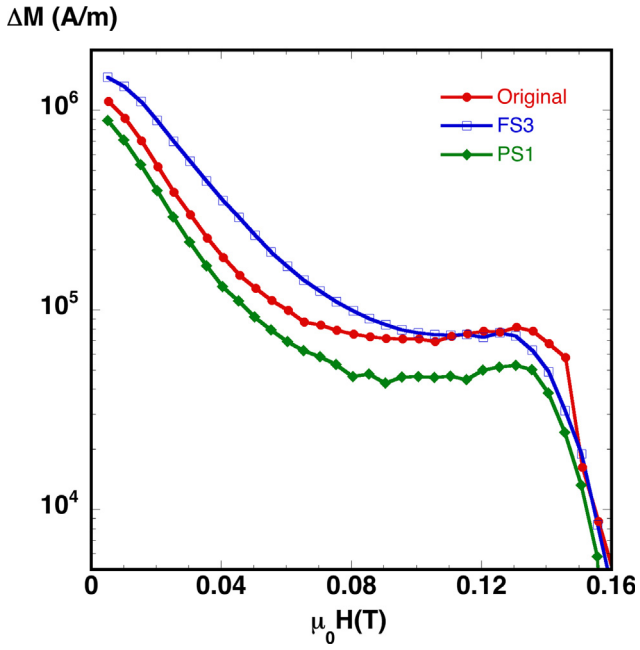

Fig. 6. Magnetic field dependence of the width of the magnetization hysteresis loops, $\Delta M(H)$, measured at 7 K for 25 μm-thick Nb samples: FS3 (processed with the fs n-IR), PS1 (processed ps UV laser) and original (non-treated). The laser conditions are collected in Table 2.

CRediT authorship contribution statement

A. Cubero: Investigation, Formal analysis, Writing - original draft. **E. Martínez:** Methodology, Investigation, Supervision, Writing - review & editing, Project administration. **L.A. Angurel:** Conceptualization, Methodology, Resources, Investigation, Writing - review & editing, Project administration. **G.F. de la Fuente:** Conceptualization, Methodology, Resources, Writing - review & editing. **R. Navarro:** Conceptualization, Writing - review & editing. **H. Legall:** Resources, Writing - review & editing. **J. Krüger:** Resources, Writing - review & editing, Project administration. **J. Bonse:** Investigation, Software, Resources, Methodology, Writing - review & editing, Project administration.

Declaration of Competing Interest

The authors declare that they have no known competing financial interests or personal relationships that could have appeared to influence the work reported in this paper.

Acknowledgements

The authors gratefully acknowledge the financial support from MINECO-AEI-FEDER (project ENE2017-83669-C4-1) and from Gobierno de Aragón "Construyendo Europa desde Aragón" (research group T54_17R). Authors also would like to acknowledge the use of Servicio General de Apoyo a la Investigación-SAI, Universidad de Zaragoza.

References

[1] H.M. van Driel, J.E. Sipe, J.F. Young, Laser-induced periodic surface structure on solids: a universal phenomenon, Phys. Rev. Lett. 49 (1982) 1955–1958.
[2] J. Bonse, S. Höhm, S.V. Kirner, A. Rosenfeld, J. Krüger, Laser-induced periodic surface structures – a scientific evergreeen, IEEE J. Sel. Top. Quant. Electron. 23 (2017) 9000615.
[3] Y.M. Andreeva, V.C. Luong, D.S. Lutoshina, O.S. Medvedev, V.Yu. Mikhailovsdii, M.K. Moskvin, G.V. Odintsova, V.V. Romanov, N.N. Shchedrina, V.P. Veiko, Laser coloration of metals in visual art and design, Opt. Mater. Exp. 9 (2019) 1310–1319.
[4] E.I. Ageev, V.P. Veiko, E.A. Vlasova, Y.Y. Karlagina, A. Krivonosov, M.K. Moskvin, G.V. Odintsova, V.E. Pshenichnov, V.V. Romanov, R.M. Yatsuk, Controlled manostructures formation on stainless steel by short laser pulses for products protection against falsification, Opt. Exp. 26 (2018) 2117–2122.
[5] J.M. Romano, A. García-Girón, P. Penchev, S. Dimov, Triangular laser-induced submicron textures for funtionalising stainless steel surfaces, Appl. Surf. Sci. 440 (2018) 162–169.
[6] A.H.A. Lutey, L. Gemini, L. Romoli, G. Lazzini, F. Fuso, M. Faucon, R. Kling, Towards laser-textured antibacterial surfaces, Sci. Rep. 8 (2018) 10112.
[7] L. Jiang, W. Han, X. Li, Q. Wang, F. Meng, Y. Li, Crystal orientation dependence of femtosecond laser-induced periodic surface structure on (100) silicon, Opt. Lett. 39 (2014) 3114–3117.
[8] X. Sedao, C. Maurice, F. Garrelie, J.P. Colombier, S. Reynaud, R. Query, F. Pigeon, Influence of crystal orientation on the formation of femtosecond laser-induced periodic surface structures and lattice defects accumulation, Appl. Phys. Lett. 104 (2014) 171605.
[9] C. Li, G.H. Cheng, J.P. Colombier, N. Faure, S. Reynaud, H. Zhang, D. Jamon, R. Stoian, Impact of evolving surface nanoscale topologies in femtosecond laser structuring of Ni-based superalloy CMSX-4, J. Opt. 18 (2016) 015402.
[10] J. Eisenstein, Superconducting elements, Rev. Mod. Phys. 26 (1954) 277–291.
[11] P. Kumar, High purity niobium for superconducting applications, Jour. Less Com. Met. 139 (1988) 149–158.
[12] S. Casalbuoni, E.A. Knabbe, J. Kötzler, L. Lilje, L. von Sawilski, P. Schmüser, B. Steffen, Surface superconductivity in niobium for superconducting RF cavities, Nucl. Instrum. Meth. Phys. Res. A 538 (2005) 45–64.
[13] Z.-H. Sung, A. Dzyuba, P.J. Lee, D.C. Larbalestier, L.D. Cooley, Evidence of incomplete annealing at 800 °C and the effects of 120 °C baking on the crystal orientation and the surface superconducting properties of cold-worked and chemically polished Nb, Supercond. Sci. Technol. 28 (2015) 075003.
[14] H. Padamsee, 50 years of success for SRF accelerators—a review, Supercond. Sci. Technol. 30 (2017) 053003.
[15] N. Singh, M.N. Deo, M. Nand, S.N. Jha, S.B. Roy, Raman and photoelectron spectroscopic investigation of high-purity niobium materials: oxides, hydrides, and Hydrocarbons, J. Appl. Phys. 120 (2016) 114902.
[16] V.V. Lennikov, B. Özkurt, L.A. Angurel, A. Sotelo, B. Özçelik, G.F. de la Fuente, Microstructure and transport properties of Bi-2212 prepared by CO_2 laser line scanning, J. Supercond. Novel Magn. 26 (2013) 947–952.
[17] K. Ozturk, C. Aksoy, L.A. Angurel, B. Savaskan, E. Martinez, A. Badía-Majós, G.F. de la Fuente, B. Guner, C.E.J. Dancer, S. Celik, IR laser line scanning treatments to improve levitation forces in $MgTi_{0.06}B_2$ bulk materials, J. Alloys Compds. 811 (2019) 151966.
[18] M. García-Lechuga, D. Puerto, Y. Fuentes-Edfuf, J. Solis, J. Siegel, Ultrafast moving-spot microscopy: birth and growth of laser-induced periodic surface structures, ACS Photo. 3 (2016) 1961–1967.
[19] Y. Fuentes-Edfuf, J.A. Sánchez-Gil, C. Florian, V. Giannini, J. Solis, J. Siegel, Surface plasmon polaritons on rough metal surfaces: role in the formation of laser-induced periodic surfaces structures, ACS Omega 4 (2019) 6939–6946.
[20] T.T.D. Huynh, N. Semmar, Dependence of ablation threshold and LIPSS formation on copper thin films by accumulative UV picosecond laser shots, Appl. Phys. A 116 (2014) 1429–1435.
[21] A. Talbi, C. Tchiffo Tameko, A. Stolz, E. Millon, C. Boulmer-Leborgne, N. Semmar, Nanostructuring of titanium oxide thin film by UV femtosecond laser beam: From one spot to large surfaces, Appl. Surf. Sci. 418 (2017) 425–429.
[22] C. Acosta-Zepeda, P. Saavedra, J. Bonse, E. Haro-Poniatowski, Modelling of silicon topographies induced by single nanosecond laser pulse induced melt-flows, J. Appl. Phys. 125 (2019) 175101.
[23] M. Gedvilas, G. Raciukaitis, V. Kucikas, K. Regelskis, Driving forces for self-organization in thin metal films during their partial ablation with a cylindrical focused laser beam, AIP Conf. Proc. 1464 (2012) 229–243.
[24] C.P. Bean, Magnetization of high-field superconductors, Rev. Mod. Phys. 36 (1964) 31–39.
[25] E.H. Brandt, Electric field superconductors with rectangular cross section, Phys. Rev. B 52 (1995) 15442–15457.
[26] U. Hermens, S.V. Kirner, C. Emonts, P. Comanns, E. Skoulas, A. Mimidis, H. Mescheder, K. Winands, J. Krüger, E. Stratakis, J. Bonse, Mimicking lizard-like surface structures upon ultrashort laser pulse irradiation of inorganic materials, Appl. Surf. Sci. 418 (2017) 499–507.
[27] C. Kunz, J.F. Bartolomé, E. Gnecco, F.A. Müller, S. Gräf, Selective generation of laser –induced periodic surface structures on Al_2O_3-ZrO_2-Nb composites, Appl. Surf. Sci. 434 (2018) 582–587.